Wrinkled Graphene Cages as Hosts for High-Capacity Li Metal Anodes Shown by Cryogenic Electron Microscopy

Hansen Wang,[†] Yuzhang Li,[†] Yanbin Li,[†] Yayuan Liu,[†] Dingchang Lin,[†] Cheng Zhu,[†] Guangxu Chen,[†] Ankun Yang,[†] Kai Yan,[†] Hao Chen,[†] Yangying Zhu,[†] Jun Li,[†] Jin Xie,[†] Jinwei Xu,[†] Zewen Zhang,[†] Rafael Vilá,[†] Allen Pei,[†] Kecheng Wang,[†] and Yi Cui*[,†,‡]

[†]Department of Materials Science and Engineering, Stanford University, Stanford, California 94305, United States

[‡]Stanford Institute for Materials and Energy Sciences, SLAC National Accelerator Laboratory, 2575 Sand Hill Road, Menlo Park, California 94025, United States

ABSTRACT: Lithium (Li) metal has long been considered the "holy grail" of battery anode chemistry but is plagued by low efficiency and poor safety due to its high chemical reactivity and large volume fluctuation, respectively. Here we introduce a new host of wrinkled graphene cage (WGC) for Li metal. Different from recently reported amorphous carbon spheres, WGC show highly improved mechanical stability, better Li ion conductivity, and excellent solid electrolyte interphase (SEI) for continuous robust Li metal protection. At low areal capacities, Li metal is preferentially deposited inside the graphene cage. Cryogenic electron microscopy characterization shows that a uniform and stable SEI forms on the WGC surface that can shield the Li metal from direct exposure to electrolyte. With increased areal capacities, Li metal is plated densely and homogeneously into the outer pore spaces between graphene cages with no dendrite growth or volume change. As a result, a high Coulombic efficiency (CE) of ~98.0% was achieved under 0.5 mA/cm^2 and 1−10 mAh/cm^2 in commercial carbonate electrolytes, and a CE of 99.1% was realized with high-concentration electrolytes under 0.5 mA/cm^2 and 3 mAh/cm^2. Full cells using WGC electrodes with prestored Li paired with Li iron phosphate showed greatly improved cycle lifetime. With 10 mAh/cm^2 Li metal deposition, the WGC/Li composite anode was able to provide a high specific capacity of ~2785 mAh/g. With its roll-to-roll compatible fabrication procedure, WGC serves as a highly promising material for the practical realization of Li metal anodes in next-generation high energy density secondary batteries.

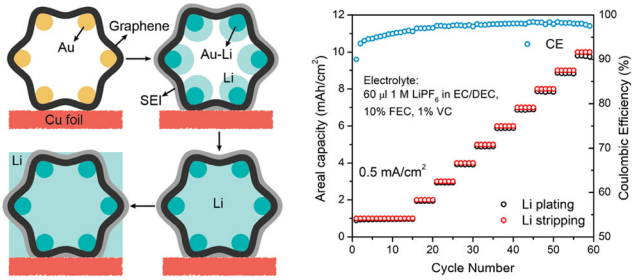

KEYWORDS: *Li metal anode, wrinkled graphene cage, Coulombic efficiency, cryo-EM*

Lithium (Li)-ion batteries utilizing graphite anodes and Li transition-metal oxide cathodes are being widely used for electric vehicles and various portable electronics.[1,2] However, the limited theoretical capacity for both anode and cathode materials cannot keep up with the increasing demand for high energy density batteries. Among all the possible alternative anodes, Li metal is the ultimate choice.[3,4] This is due to its highest theoretical capacity (3860 mAh/g) and its lowest electrode potential (−3.04 V versus standard hydrogen electrode). Unfortunately, commercializing the Li metal anode still remains a critical challenge, mainly attributed to its low cycling efficiency.[3] The corrosive battery electrolyte decomposes upon contact with Li metal during battery operation, forming a solid electrolyte interphase (SEI). If this SEI layer is mechanically strong and chemically stable, it will suppress or, in an ideal case, prevent fresh Li metal from further reacting with the electrolyte. However, because of its "hostless" nature, Li metal deposition and stripping causes a huge relative volume change that can easily crack the SEI, which leads to an increased local ion flux and dendritic Li metal deposition (Figure 1e−g). These Li metal dendrites not only increase the risk of short circuits and fires but also greatly increase the surface area of Li metal, leading to heavy consumption of both Li and electrolyte during each cycle as well as the formation of dead Li (Figure 1h). This is the major reason for low Coulombic efficiency (CE) and fast capacity decay, which prevent the practical realization of Li metal anode.

To achieve homogeneous Li metal deposition and high CE, various methods have been explored, including engineering of the SEI and screening different electrolyte chemistries. Artificial thin films, including two-dimensional materials,[5] amorphous carbon,[6] polymers,[7,8] and ceramics,[9−12] were synthesized to improve the chemical stability and mechanical

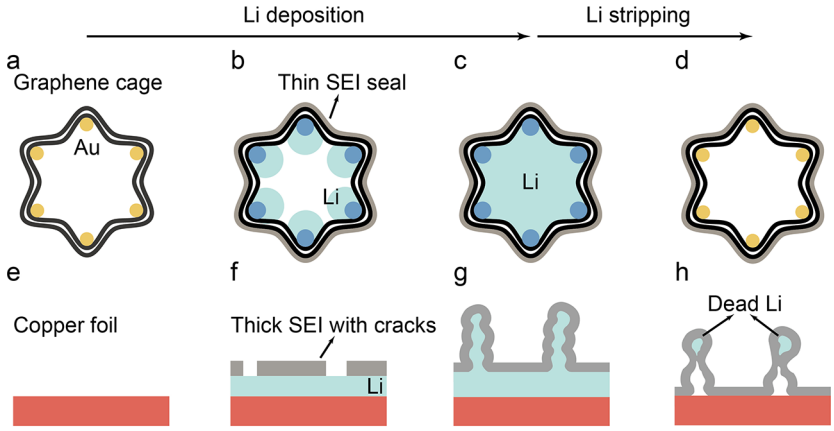

Figure 1. Comparison between WGC and copper foil during Li deposition and stripping. (a) Pristine WGC. (b and c) WGC after various amounts of Li deposition. (d) WGC after stripping all the Li metal away. (e) Copper foil. (f and g) Copper foil after various amounts of Li deposition. (h) Copper foil after stripping Li metal away.

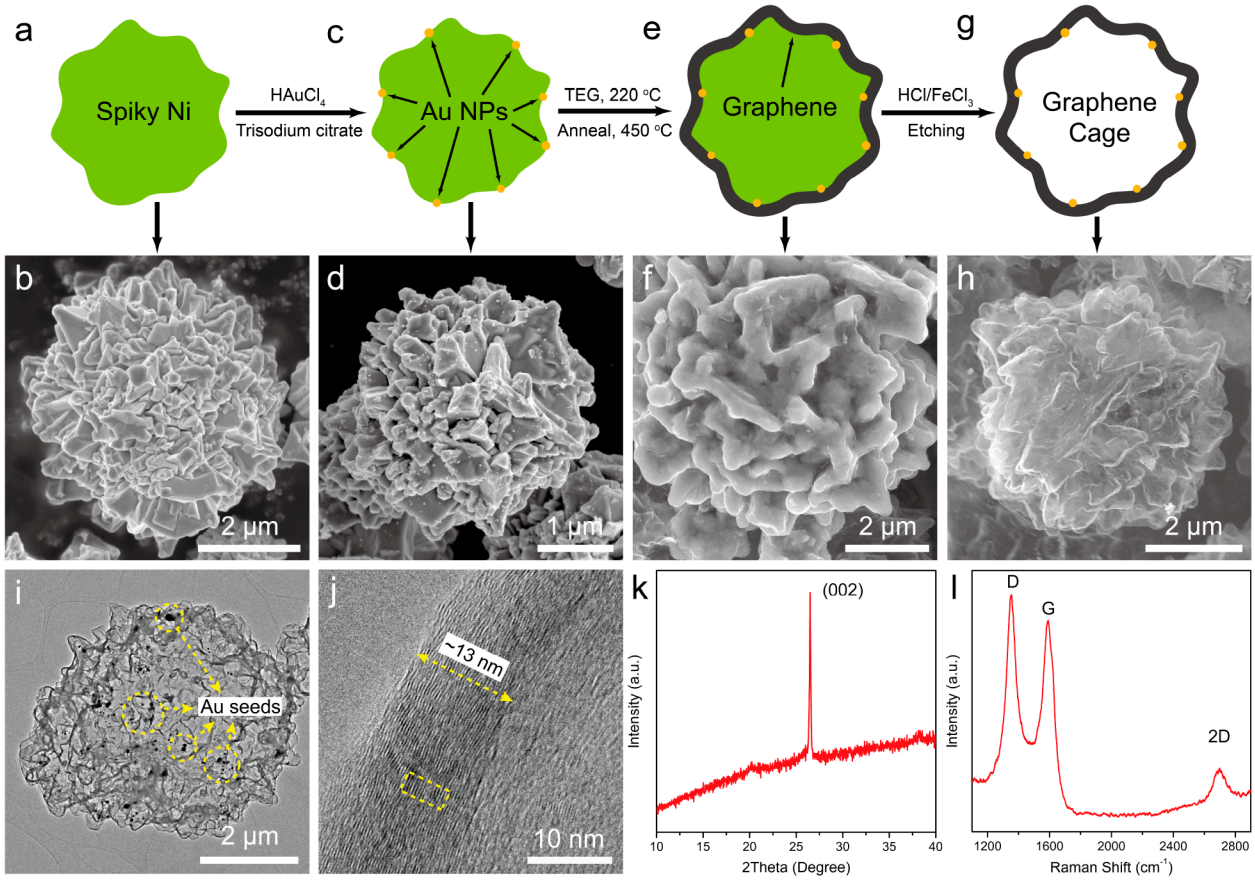

Figure 2. Fabrication and characterizations of WGC. (a) Schematic and (b) SEM image of the spiky nickel powder used as precursor. (c) Schematic and (d) SEM image of spiky nickel powder coated with gold nanoparticles. (e) Schematic and (f) SEM image of spiky nickel after graphene growth on the surface. (g) Schematic and (h) SEM image of WGC with gold nanoparticles on the inner surface after etching away the Ni. (i) TEM image of a WGC. (j) High-resolution TEM image of the graphene cage. (k) XRD pattern of WGC indicating graphitic nature of the cages. (l) Raman spectrum of WGC showing graphitic yet defective nature of the cages.

robustness of the SEI. Introducing electrolyte additives such as halogenated salt,[13] lithium nitrate,[14] polysulfides,[15] fluoroethylene carbonate (FEC),[16,17] ionic liquids,[18] or nanodiamonds[19] or increasing salt concentration[20−22] were shown to change the local chemical environment for charge transfer and promote better deposition morphology. These efforts successfully improved the CE of Li metal anodes to over 98% in carbonate electrolyte systems. However, these methods fail to address the hostless nature of Li metal, meaning that Li metal is plated and stripped without any physical confinement. Thus, it has not been possible to achieve high CE of Li metal at high areal capacities (i.e., 10 mAh/cm^2). For example, 10 mAh/cm^2 of Li metal has a thickness of 50 μm/cm^2. Such large volume fluctuations during Li metal cycling compromise the SEI and cause continuous consumption of both active material and electrolyte. Recently, we introduced the idea of an artificial

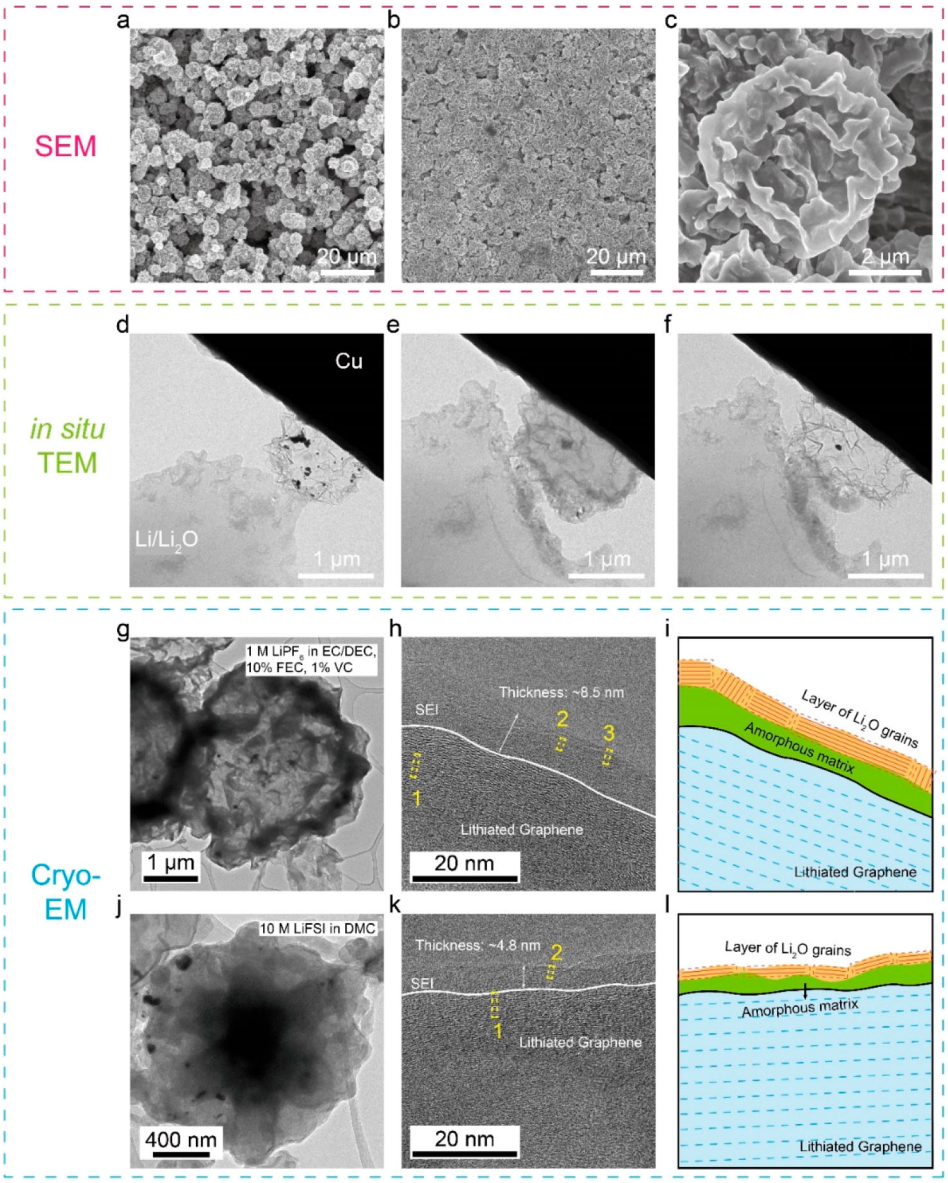

Figure 3. Characterization of WGC after low areal capacity Li metal deposition. (a) SEM image of a pristine WGC electrode. (b) SEM image and zoomed-in image (c) of a WGC electrode after depositing 1 mAh/cm^2 of Li metal. (d) In situ TEM observation of a pristine WGC. The WGC could be completely filled with Li metal during deposition (e) and fully emptied after Li metal stripping (f). (g) Cryo-EM and (h) high-resolution cryo-EM image of a WGC with 1 mAh/cm^2 of Li metal deposition using electrolyte of 1 M $LiPF_6$ in EC/DEC, 10% FEC, 1% VC. (i) Schematic of the SEI nanostructure observed on the surface of the WGC in panel h. (j) Cryo-EM and (k) high-resolution cryo-EM image of a WGC with 1 mAh/cm^2 of Li metal deposition using electrolyte of 10 M LiFSI in DMC. (l) Schematic of the SEI nanostructure observed on the surface of the WGC in panel k. Cryo-EM is able to preserve the sensitive battery material and show that the SEI is much thinner on the WGC than on pure Li metal, leading to the increased CE.

"host" for Li metal to prevent volume fluctuation during Li metal cycling with reduced graphene oxides[23] and seeded hollow carbon spheres.[24] Subsequently, various other porous structures, including carbon-based (carbon fiber,[25−28] graphitic carbon foam,[29] carbon nanotube,[30] carbon spheres with coating[31]), polymer-based (PI fiber,[32] PAN fiber[33]), metal-based (high surface area copper,[34] nickel foam[35]), and single-step overlithiation-induced[36,37] matrices, were fabricated. These structures are capable of reducing the electrode volume change during cycling and the local current density, leading to lower overpotentials during charge−discharge and a more stable SEI. Despite these advantages, "host" structures still have some limitations for practical applications. Take the recently reported amorphous carbon spheres with gold seeds[24] and LiF coating[31] as an example; they are mainly limited by three drawbacks. First, they usually show poor mechanical strength due to their amorphous nature, leading to broken spheres during cell crimpling or electrode calendaring thus losing protection for Li metal. Second, the amorphous shell has rather low Li ion conductivity, resulting in higher impedance for Li ion to transfer inside the cage and plate out as Li metal. Finally, amorphous carbon spheres can hardly handle Li deposition capacity higher than 2 mAh/cm^2, possibly because of the poor Li metal deposition quality outside the spheres. Even with other Li metal host structures with prestored Li metal, performances are still not sufficient for practical next-

generation Li metal battery chemistries (Li−S, Li−O_2), where a high loading of over 3 mAh/cm^2 and at lifetimes of at least 300 cycles without obvious capacity decay are needed. Thus, a host structure that can handle high areal capacity with further improved CE would represent a significant advance.

Herein, we introduce a seeded wrinkled graphene cage (WGC) structure (Figure 1a) as a novel host. WGC are fabricated through low-temperature graphene synthesis using spiky nickel powder as a template. Li metal can be preferentially plated into the cages through the defects/pinholes on the graphene shell[5,38−40] because of the reduced nucleation overpotential on the gold nanoparticles embedded on the inner surface (Figure 1b,c). After the Li metal is stripped away, the SEI will be maintained because of the well-defined structure of the WGC (Figure 1d). WGC differentiates from amorphous carbon spheres[24,31] in three aspects. First, WGC offers excellent mechanical strength, which will be shown by *in situ* transmission electron microscopy (*in situ* TEM). It can not only be compressed but also be sheared and restore its original shape. This minimizes cage shattering during cell crimpling, promoting much more robust Li metal protection. Second, the high-quality graphitic structure of the shell enables Li ion intercalation and transportation, reducing the impedance for Li metal plating into the cages. Shown by cryo-electron microscopy (cryo-EM), the graphene shell also promotes high quality thin SEI that perfectly seals the defects/pinholes on the cages (Figure 1b), which minimizes contact between the electrolyte and Li plated inside. Furthermore, because of the wrinkled high surface area morphology of the WGC, we are able to demonstrate a dual-stage Li plating mode using focused ion beam (FIB) cutting, which enables excellent CE with ultrahigh areal capacities. Typically, a ∼60 μm thick, ∼1 mg/cm^2 loading WGC electrode is capable of achieving a high CE over 98% at areal capacities from 1 mAh/cm^2 to 10 mAh/cm^2 in a commercial carbonate electrolyte system with additives. With the usage of high concentration electrolyte (HCE), the CE is further improved to 99.1% under 0.5 mA/cm^2 and 3 mAh/cm^2. A full cell with Li iron phosphate (LFP) cathodes using WGC can be cycled for over 340 cycles without obvious capacity decay. With its fabrication method which is highly compatible with the roll-to-roll industrial procedure, WGC is a highly promising candidate for large-scale, high specific capacity, and high-efficiency Li metal anodes.

Results. *Synthesis of WGC.* Figure 2 illustrates the fabrication procedure and basic characterizations of the WGC. A commercial spiky nickel (Ni) powder was used as the template for graphene growth (Figure 2a). Figure 2b shows the scanning electron microscopy (SEM) image of the Ni template. A wrinkled texture can be clearly observed, leading to a similar shape of the resulting WGC. Later, chloroauric acid hydrate was reduced by trisodium citrate in water with suspended spiky Ni powder. As a result, gold nanoparticles precipitated onto Ni particles, which is shown in the schematic (Figure 2c) and SEM image (Figure 2d). Afterwards, we utilized a previously reported Ni carburization−carbon segregation method for low-temperature graphene growth.[41,42] Typically, the Ni powder coated with gold nanoparticles was stirred in triethylene glycol (TEG) at 200 °C overnight, followed by annealing in a tube furnace under argon (Ar) atmosphere at 600 °C. Layers of graphene form on the outer surface of the Ni powder, which is shown in the schematic (Figure 2e) and SEM image (Figure 2f). Finally, the Ni powder coated with graphene was etched in 1 M/1 M $FeCl_3$/HCl solution overnight to fully remove the Ni inside, forming the final WGC product with diameter 2−5 μm (Figure 2g,h). Figure 2i shows a TEM image of a WGC. A hollow structure without Ni can be clearly observed. Also we can see gold nanoparticles dispersed inside the graphene shell. Energy-dispersive X-ray spectroscopy (EDS) results (Figure S1) show negligible amounts of Ni residue and high intensity of carbon and gold. High-resolution TEM (Figure 2j) shows the layered structure of the graphene shell with a thickness of ∼13 nm. A lattice spacing of ∼0.35 nm in the yellow box was measured for the shell (Figure S2a), which is slightly larger than the reported value for graphite (∼0.335 nm).[43,44] This deviation may come from the low-temperature fabrication procedure, which would possibly lead to higher disorder and loose packing.[45] X-ray diffraction results in Figure 2k show a high-intensity (002) peak (2θ = 27°), further confirming the crystalline structure of the graphene shell. Figure 2i is the Raman spectrum of WGC, where a high-intensity D peak can be observed, indicating the existence of a large amount of defects on the cage which facilitate Li ion transfer through the graphene shell for Li metal deposition.

Characterization of WGC Electrodes after Li Deposition. Figure 3a illustrates the SEM image of a pristine slurry-coated WGC electrode. After 1 mAh/cm^2 deposition of Li metal, the morphology of the electrode can be seen in Figure 3b. A much denser surface pattern can be observed, probably because of the pressure exerted during coin cell assembly. No Li dendrite growth can be observed over a large area, indicating the plating of Li metal within the cages. Figure 3c shows an enlarged SEM image of a WGC. It is clear that the cage did not expand and maintains its original shape. Expanding an already-filled cage through additional Li deposition would require a large overpotential, which would instead cause Li metal to be deposited outside the cage. As a result, a stable and interconnected WGC framework covered with SEI forms for Li metal plating at low areal capacities. To confirm Li metal is indeed deposited preferentially into the cage, in situ imaging was done using a microscale electrochemical cell inside the TEM to show the process. The specific setup follows previous work.[24,42] Figure 3d shows the initial state of a WGC in contact with copper substrate and Li metal coated with Li oxide (Li_2O) as solid electrolyte. After current was applied to deposit Li metal, it can be clearly observed in Video S1 that Li first alloyed with gold nanoparticles embedded inside the cage, then nucleated, and gradually grew large until all of the cage was filled (Figure 3e). Afterward, Li metal was stripped away from the cage (Video S2), returning the cage to its original shape with gold nanoparticles inside (Figure 3f).

To characterize the SEI nanostructure and Li metal deposition within WGC in a real battery, we used cryo-electron microscopy (cryo-EM), which was recently pioneered to characterize reactive and sensitive battery materials preserved in their electrochemical state without damaging the sample.[46] Here, samples were characterized after 1 mAh/cm^2 Li deposition in both electrolyte system A (1 M lithium hexafluorophosphate ($LiPF_6$) in 1:1 ethylene carbonate/diethyl carbonate (EC/DEC) with 10 wt % FEC and 1 wt % vinylene carbonate (VC) as additives) and electrolyte system B (10 M lithium bis(fluorosulfonyl)imide (LiFSI) in dimethyl carbonate (DMC)). Figure 3g shows a cryo-EM image of a WGC after Li metal deposition in electrolyte system A. The WGC surface appears darker in contrast (Figure 2i), indicating the formation of a SEI that contains elements with higher

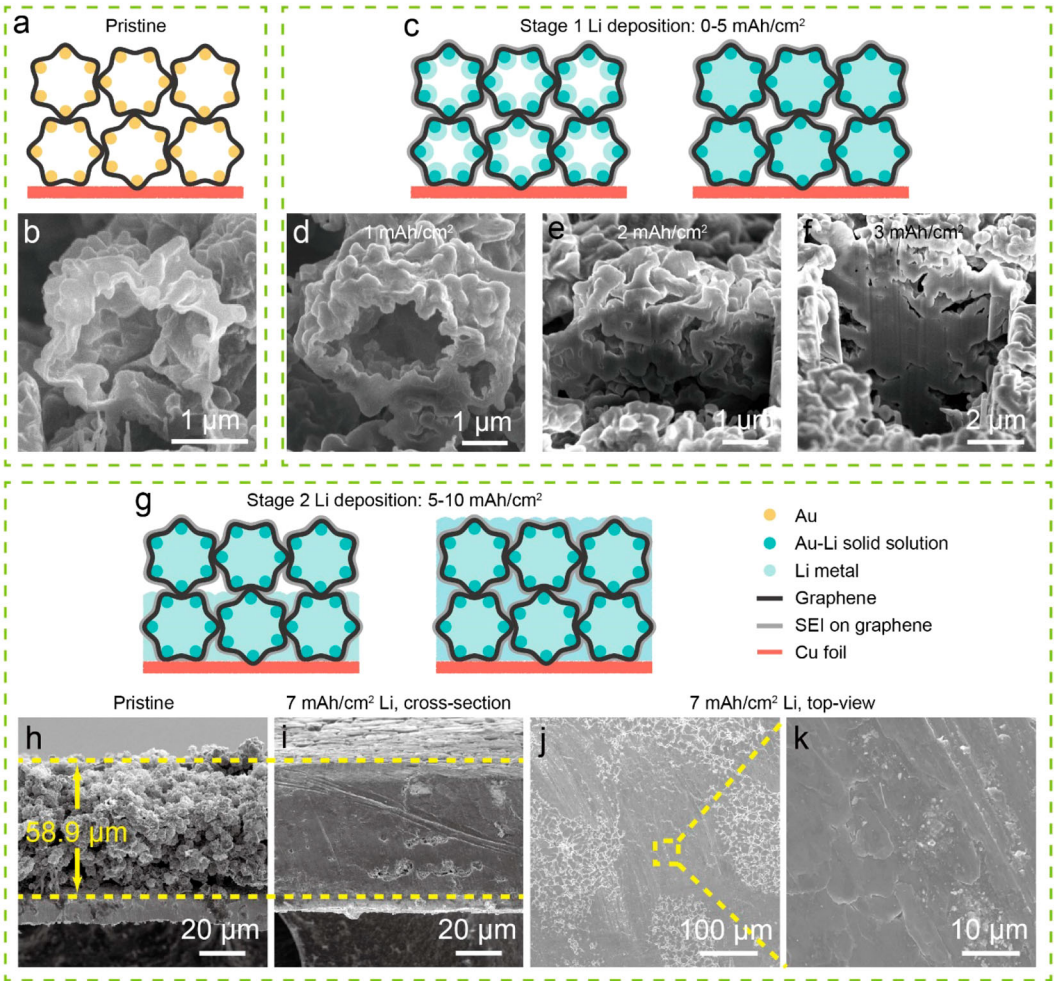

Figure 4. Schematic and characterization of WGC electrode during two stages of Li metal plating. Schematic (a) and SEM image (b) of FIB cut pristine WG and schematic (c) and SEM image of WGC after Li deposition of 1 mAh/cm^2 (d), 2 mAh/cm^2 (e), and 3 mAh/cm^2 (f). Schematic of WGC under high areal capacity Li deposition of 5−10 mAh/cm^2. (g) SEM image of cross section of a pristine WGC electrode (h) and electrode after 7 mAh/cm^2 Li metal deposition (i). SEM image of the top view of a electrode after 7 mAh/cm^2 Li metal deposition (j and k). All the above depositions were done under current density of 0.5 mA/cm^2.

atomic number. Furthermore, the interior of the WGC appears lighter in contrast, suggesting the deposition of Li metal within the cage was successful in a coin cell configuration. Figures 3h and S4 show the high-resolution image of the graphene cage after Li deposition. Graphene lattice expanded to about 0.46 nm in the region of yellow box 1, as is shown in Figure S2b. This indicates that the WGC shell can be lithiated. However, the lattice spacing deviates from previously reported lithiated graphite results[43−45] of ∼0.37 nm. Because of the highly defective and wrinkled structure of the cage, we speculate that strain inside the shell after Li ion intercalation as well as the tiny amount of Li metal nuclei between the graphene layers below 0 V vs Li/Li$^+$ might lead to further expanding the lattice. On top of the lithiated graphene cage, a uniform layer of SEI can be observed. Crystalline domains in boxes 2 and 3 at the outer surface of the SEI in Figure 3h are both measured to match the lattice of Li_2O (Figure S2c,d). Similar grains cover most of the outer layer of the SEI, while the inner part of the SEI appears to be mainly composed of amorphous polymer components (Figure 3i). This multilayer structure matches the previously reported SEI model of Li metal in carbonate electrolyte with FEC additive.[40] Significantly, the thickness of the SEI on lithiated graphene cage (∼8.5 nm) is much smaller than on Li metal (∼17 nm), which indicates less Li and electrolyte consumption for SEI formation. After Li deposition in electrolyte system B, the morphology of the cage appears to be similar (Figure 3j). In the high-resolution image (Figures 3k and S5), the lattice spacing of lithiated graphene shell is measured to be 0.363 nm (Figure S3a), showing a much mitigated expansion. A multilayered structure can be also observed (Figure 3l) with Li_2O outer layer (Figure S3b) and polymerized inner layer in system B. Note that the SEI thickness is even further reduced in this electrolyte system, which is only around 4.8 nm. This is most likely because in system B, graphene surfaces are mostly exposed to anions instead of solvent molecules because of the super high salt concentration. The anions generally are less reactive with respect to reduction compared to aprotic solvents like DMC,[20] leading to a further reduced SEI thickness. Unlike bare Li metal, the shape of WGC can be maintained during subsequent cycling with minimum volume fluctuation and shape variation, and this will lead to a very stable SEI on the WGC, preventing solvent leakage into the cage and continuous corrosion of Li metal.

Plating of Li metal onto the WGC electrode can be separated into two stages according to the areal deposition

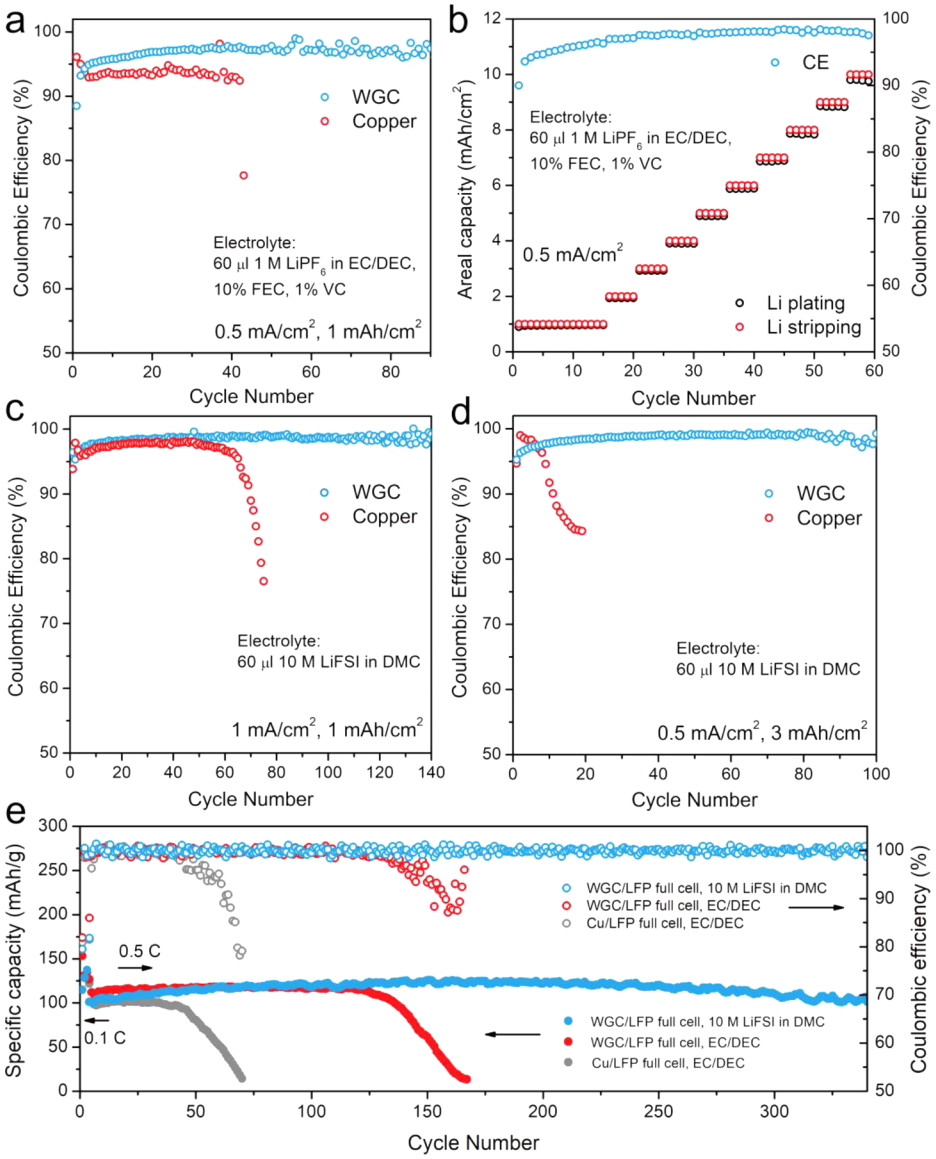

Figure 5. Electrochemical testing results of WGC electrodes. CE comparison between WGC electrodes and bare copper under 0.5 mA/cm^2 and 1 mAh/cm^2 (a) and CE of WGC electrodes under 0.5 mA/cm^2 and various areal capacities from 1 mAh/cm^2 to 10 mAh/cm^2 (b) in 1 M $LiPF_6$ in EC/DEC, 10% FEC, 1% VC electrolyte. CE comparison between WGC electrodes and bare copper under 1 mA/cm^2 and 1 mAh/cm^2 (c) and 0.5 mA/cm^2 and 3 mAh/cm^2 (d) in 10 M LiFSI in DMC electrolyte. (e) Full cell performance comparison between WGC electrodes and bare copper foil with 6 mAh/cm^2 electrodeposited Li metal under different electrolyte systems. LFP loading ≈ 9 mg/cm^2.

capacity. Morphology of the pristine WGC electrode and a WGC cage are demonstrated in panels a and b of Figure 4, respectively. A FIB was used to cut WGC open to observe its interior. A thin shell of graphene can be observed, and the cage is totally hollow (Figure 4b) before Li plating. After deposition of 1 mAh/cm^2 of Li metal, the shell became thicker (Figure 4d) because of the expanded lattice and SEI formation. Bulk Li metal started to form, but the cage still had large empty spaces. With 2 mAh/cm^2 Li metal deposition, the cages were half filled with Li metal (Figure 4e). After deposition of 3 mAh/cm^2 Li metal, it was clear that the cages were almost fully filled with Li metal (Figure 4f). Note that not all the cages were fully filled at areal loading of 3 mAh/cm^2, leaving some more spaces inside the cages for further Li metal deposition. As a result, we classify Li plating with an areal capacity of 0−5 mAh/cm^2 into stage 1 deposition, where Li metal first alloys with gold nanoparticles forming solid solution and then precipitates inside the cage until each cage is full (Figure 4c). Afterward, Li metal started to fill outer pore spaces in the WGC electrode. Figure 4h shows that a pristine WGC electrode had a thickness of ∼58.9 μm. After 7 mAh/cm^2 Li metal deposition, Figure 4i shows that the WGC electrode was densely filled with Li metal and maintained the same thickness very well; 7 mAh/cm^2 of pure Li metal corresponds to ∼35 μm thickness. This means most of the interior and exterior pores of the WGC electrode were filled with Li metal, leading to a relatively reduced exposure of Li metal to electrolyte. The morphology of the WGC electrode after 7 mAh/cm^2 Li metal deposition was further characterized (Figure 4j,k), where a smooth surface with no dendrite growth can be clearly seen. From this observation, we classify Li plating with an areal capacity of 5−10 mAh/cm^2 into stage 2 deposition, where Li metal begins plating into the empty space formed between the WGC (Figure 4g). Because of its dense and homogeneous nature, the electrode is able to suppress

volume fluctuation and dendritic growth with high loading Li metal, which possibly results in a high CE at high areal capacity.

Electrochemical Performance of WGC Electrodes. Coulombic efficiency is defined as the ratio of extracted capacity to deposited capacity. This value governs the cycle lifetime of a battery cell. Li metal CE is notoriously low, especially in commercial carbonate electrolytes, because of the huge volume change during cycling and dendrite growth. HCEs have been reported recently to manifest a much improved CE for Li metal.[20,22,47] However, they are usually plagued by high viscosity, which usually leads to bad performance under high-current densities. Here, CE performance is compared between WGC electrodes and bare copper current collectors in both electrolyte system A (commercial carbonate electrolyte with additives) and electrolyte system B (HCE with carbonate solvent). For electrolyte system A, under 0.1 mA/cm^2 and 1 mAh/cm^2, the CE of bare copper started at 95.5% and failed in approximately 20 cycles (Figure S6). In stark contrast, WGC electrodes maintained a high average CE of 98.0% from cycle 30 to cycle 70 and retained this high CE for over 90 cycles. Although the CE of WGC electrodes was initially low, it gradually increased and exceeded that of copper after 5 cycles. This is because part of the deposited Li was used to form SEI on the graphene cage surface, which is an irreversible reaction. After the cages were covered with a uniform layer of SEI, the CE of the WGC electrode stabilized and stayed at around 98.0%. When we increased the testing current density to 0.5 mA/cm^2, the CE of bare copper dropped to around 93.0% and failed after 40 cycles (Figure 5a), whereas the CE of WGC electrode stabilized at 97.5% from cycle 40 to cycle 80 (Figure 5a). At higher current density of 1 mA/cm^2, the CE of bare copper started at about 95.0% but drastically decayed to below 90.0% after only 5 cycles (Figure S7). This is possibly due to the favorable dendritic growth morphology under larger overpotential and the continuous breakdown and repairing of SEI, which leads to both Li and electrolyte loss. Under this condition, however, the WGC electrode maintained a high CE of 97.0% from cycle 40 to cycle 80 and could last for over 100 cycles. In previous work, CE was usually tested under low areal capacities (1 mAh/cm^2) for Li metal, which is far from enough for a commercial battery. Furthermore, next-generation secondary batteries (such as Li−S batteries) require a higher loading to achieve energy densities over 500 Wh/kg. Therefore, it is critical to achieve a Li metal loading of 5−10 mAh/cm^2. CE with such high cycling areal capacity has rarely been tested in carbonate electrolyte systems because the previously discussed issues are exacerbated with higher capacities. Here, we test the CE of WGC electrodes under current density of 0.5 mA/cm^2 and areal capacity from 1 mAh/cm^2 to 10 mAh/cm^2. Under these rigorous conditions, the CE was preserved at ∼98.0% (Figure 5b). Typically, at areal capacity greater than 5 mAh/cm^2, the WGC electrode enters stage 2 deposition where Li metal starts to deposit into the pore space outside of the cages. This not only suggests that Li metal was successfully protected inside the cage during stage 1 deposition but also confirms that the CE for Li metal outside the cages in stage 2 was high because of its dense and homogeneous structure with no volume fluctuation and dendrite growth. The WGC loading used here was ∼1 mg/cm^2. With 10 mAh/cm^2 Li metal deposited inside, the WGC/Li metal composite electrode would offer a high specific capacity of ∼2785 mAh/g. These results makeWGC one of the best Li metal current collector candidates with not only high specific capacity but also exceptional CE at ultrahigh areal capacities. In electrolyte system B, under 1 mA/cm^2 and 1 mAh/cm^2, bare copper foil was able to achieve a CE over 98.0% initially but decayed drastically after only 60 cycles. In contrast, WGC electrode achieved a stable CE of 99.0% for over 140 cycles (Figure 5c). Under 0.5 mA/cm^2 and 3 mAh/cm^2, copper foil was not able to work at all. However, with WGC electrodes, a stable high CE of 99.1% was observed from cycle 40 to cycle 80 (Figure 5d). We believe this indicates that the WGC electrodes successfully compensated the weakness of HCE (high viscosity) with its high surface area, making HCE capable of working at practical cycling conditions.

Finally, full cell performance using WGC electrodes and bare copper with prestored, electrodeposited Li metal paired with Li iron phosphate (LFP) was demonstrated. Here, Li areal capacity of 6 mAh/cm^2 was prestored into the WGC electrode and bare copper and LFP loading was ∼9 mg/cm^2. The cells were first activated at 0.1 C (1 C = 170 mAh/g) for 3 cycles and then cycled at 0.5 C. Figure 5e shows that in electrolyte system A, bare copper/LFP cell was able to offer a specific capacity of only ∼95 mAh/g (based on LFP mass loading) at 0.5 C. Additionally, the capacity started to decay drastically after only 40 cycles because of the complete consumption of excess Li metal. In contrast, WGC/LFP cell demonstrated a much higher specific capacity of ∼120 mAh/g at 0.5 C and lasted for more than 120 cycles. Here, the improved specific capacity comes from the reduced overpotential of WGC electrodes due to its thin uniform SEI layer and much reduced local current density compared to that of Li metal on bare copper. The increased cycle life arises from the higher CE of WGC electrodes that was shown previously. Less Li metal was consumed during each cycle; therefore, the full cell could maintain a high specific capacity for a longer time. In electrolyte system B, the WGC electrode initially showed a specific capacity of ∼100 mAh/g which gradually increased to over 120 mAh/g after long time cycling. We believe this was because a long time was needed for the highly viscous HCE to fully wet the separator and porous spaces inside the WGC electrode. With HCE, the WGC/LFP full cell was able to be cycled for over 340 cycles with tiny capacity decay, manifesting a much prolonged cycling lifetime. This is compatible with the CE testing results in the WGC/Li cell. As a conclusion, combining WGC with HCE greatly improved the CE and full cell cycling lifetime without diminishing its energy density because of the low WGC mass loading (1 mg/cm^2).

Discussion. Compared to previously reported amorphous carbon spheres used as Li metal host,[27] WGC shows much improvement in two aspects. First, WGC has much better mechanical strength than amorphous carbon because of its graphitic nature. The brittleness of an amorphous carbon sphere was previously shown.[36] In Video S3, we used a similar setup to characterize WGC behavior under shear and compression in situ. It can be observed that the WGC not only was able to resist compressive forces by completely deforming and recovering its original shape but also could resist shear forces with excellent flexibility. Furthermore, previously reported amorphous carbon spheres had diameters around 500 nm, whereas WGC has diameters from 2 to 5 μm. Such large amorphous carbon spheres will likely be damaged by mechanical deformation during slurry fabrication and calendaring, losing its protection for the Li metal. In contrast, WGC can maintain its original structure during the whole

fabrication process well, facilitating a good encapsulation for the Li metal plated inside. Second, CE testing results show that amorphous carbon sphere electrodes failed at 3 mAh/cm^2 and stage 2 Li deposition will be dendritic with low CE, while WGC can maintain high CE up to 10 mAh/cm^2 and have a dense Li deposition in stage 2. This boosts the possibility of WGC electrodes for practical use in next-generation high energy density secondary batteries.

It is interesting that stage 2 showed such dense Li metal deposition and had a high CE comparable to that of stage 1. We believe that two possible explanations might contribute to this phenomenon. First, a small amount of Li metal could still be found on the outside surfaces of the WGC electrode even under stage 1 deposition. We believe that this was caused by a few cages that were slightly damaged during the fabrication procedure. Li metal can then be directly exposed to electrolyte and grow without being confined by the cage. Ideally, if all the cages are intact, perfect seals will form and we may reach a high CE near 100.0%. Practically, however, we could achieve only around 98.0% because of the imperfection of the cage fabrication. This diminished the CE in stage 1 deposition. Second, CE in stage 2 deposition was boosted because of the existence of high surface area graphene cages. On one hand, it has been reported repeatedly that Li metal would have a much increased plating homogeneity on graphene-based structures.[23,48,49] Lithiated graphene surface may facilitate Li metal nucleation, leading to a reduced overpotential. On the other hand, the wrinkled structure greatly elevated the surface area exposed to the electrolyte, effectively reducing local current density, which would further reduce the Li plating overpotential. For both of these reasons, Li was deposited into a very dense and uniform morphology, and only the top surface was exposed to electrolyte and corroded. As a result, no matter how high an areal capacity we applied during the cycling, stage 2 deposition CE was comparable to that of stage 1. Questions are always raised when the structure has a high surface area, as it seems to consume more electrolyte and Li species to form SEI. We believe this is not a problem for WGC. The reason is because WGC has a well-defined shape, and the SEI formed will not keep breaking and repairing after the formation cycles. This point is also indicated in the CE testing results, where the CE always starts at a rather low point and stabilizes at a high value after the first few cycles.

In summary, WGC was fabricated as a practical host material for Li metal anodes. This material successfully suppressed dendrite growth and volume fluctuation during cycling. Uniform SEI formed outside the cage sealed the defects and pinholes and protected the Li metal deposited inside during stage 1. High surface area lithiated graphene facilitated further Li metal deposition outside the cages in stage 2. As a result, a high average CE of ∼98.0% was achieved for cycling capacity up to 10 mAh/cm^2 in commercial electrolyte with additives. Under such high Li metal loadings, the WGC electrodes had a high specific capacity of ∼2785 mAh/g. With the usage of HCE, the CE was further improved to 99.1% with 3 mAh/cm^2 areal capacity. Full cells using WGC with prestored Li metal paired with LFP cathode showed higher specific capacity and much increased cycle life in comparison to that with bare copper. With HCE, the full cell was able to be cycled for 340 cycles without obvious capacity decay. Most importantly, the fabrication procedure of WGC electrodes was highly compatible to roll-to-roll processes in current battery industries. These properties enabled WGC to be a highly promising Li metal anode host material for next-generation higher energy density secondary batteries.

Methods. *Fabrication of WGC.* A 2 g sample of spiky nickel powder (Novamet) was dispersed in 150 mL of deionized water, and 1 mL of 1 M trisodium citrate (Sigma-Aldrich) solution was added. Afterward, 2 mL of 6.75 mM $HAuCl_4$ solution was added under vigorous stirring. The reaction was kept at room temperature for 10 min. Spiky nickel powder was then filtered and dried in a vacuum oven for 4 h. Later, the powder was dispersed in 200 mL of triethylene glycol (Sigma-Aldrich), and the mixture was stirred at 250 °C overnight. The resulting suspension was centrifuged and washed with ethanol 5 times. The resulting powder was dried in a vacuum oven overnight. The dried powder was placed in a tube furnace with the following temperature profile: heat to 100 °C at 2 °C min^{-1}; heat to 450 °C at 20 °C min^{-1}; hold temperature at 450 °C for 1 h. An Ar flow rate of 80 sccm was maintained throughout the annealing process. The resulting graphene-covered nickel powder was etched in 1 M/1 M $FeCl_3$/HCl solution overnight and then filtered, washed, and dried in a vacuum oven.

Characterizations. SEM images were taken using a FEI XL30 Sirion scanning electron microscope at an acceleration voltage of 5 kV. For the characterization of stage 1 deposition, a FIB was used to cut open the cages, which was carried out using an FEI Strata 235DB dual-beam FIB/SEM with gallium ion source. XRD patterns were recorded on a PANalytical X'Pert instrument. TEM images for pristine WGC were taken using an FEI Titan 80-300 environmental (scanning) transmission electron microscope (E(S)TEM) operated at 300 kV. Cryo-EM and in situ TEM characterizations followed previously reported procedures.[42,46,50]

Electrochemistry. WGC electrode was made using a conventional doctor blade-casting procedure. Typically, WGC powder and polyvinylidene fluoride (PVDF, Kynar HSV 900) binder with a mass ratio of 9:1 were dispersed in *N*-methyl-2-pyrrolidone (NMP) in the absence of any conductive additives, and the mixture was stirred for 12 h. The suspension was then casted onto a 15 μm thick copper foil and dried at 60 °C in a vacuum oven for 6 h. The electrode was cut into 1 cm^2 circular disks with total mass loading of ∼1 mg/cm^2. All disk electrodes were placed inside an Ar-filled glovebox with sub-ppm oxygen and water levels (Vigor Tech) for at least 24 h before use. LFP electrodes were fabricated by doctor blade-casting LFP powder (MTI Inc.), Ketjenblack (EC-300J; AkzoNobel), and PVDF (8:1:1) suspension onto copper foil. The mass loading of active LFP was ∼9 mg/cm^2. For CE testing, either WGC electrode or copper foil was assembled into type 2032 coin cells with a polymer separator (Celgard 2250) and Li metal (Alfa Aesar) as counter/reference electrode. For full cell testing, either WGC electrode or copper foil were paired with Li foil to electrochemically deposit Li metal. Afterward, the cells were disassembled and the electrodes with prestored Li metal were then paired with LFP electrodes as cathode. Either electrolyte system A (1.0 M $LiPF_6$ in 89 vol % 1:1 w/w ethylene carbonate/diethyl carbonate (BASF Selectilyte LP40) with 10 vol % fluoroethylene carbonate and 1 vol % vinylenecarbonate (Novolyte Technologies)) or B (10.0 M LiFSI (Oakwood Chemical, 99%) in dimethyl carbonate (Sigma-Aldrich, 99.9%)) were used in the battery testings. For half and full cells, 60 and 80 μL of electrolyte were used, respectively. All cell measurements were carried out using a LAND 8-channel battery tester.

AUTHOR INFORMATION

Corresponding Author

*E-mail: yicui@stanford.edu.

ORCID

Hansen Wang: 0000-0002-6738-1659
Yuzhang Li: 0000-0002-1502-7869
Yanbin Li: 0000-0002-5285-8602
Dingchang Lin: 0000-0002-9354-5952
Ankun Yang: 0000-0002-0274-4025
Hao Chen: 0000-0002-2852-0070
Jin Xie: 0000-0002-6270-1465
Allen Pei: 0000-0001-8930-2125
Yi Cui: 0000-0002-6103-6352

Author Contributions

H.W. and Yuzhang Li contributed equally to this work. H.W. and Yuzhang Li designed the experiment. H.W. conducted material synthesis, SEM-FIB characterization, and electrochemical testing. Yuzhang Li, Yanbin Li, G.C., and R.V., conducted TEM characterizations. D.L., Yayuan Liu, C.Z., H.C., Y.Z., J.L., Jinwei Xu, Z.Z., Jin Xie, A.P., and K.W. participated in electrochemical testing. A.Y. conducted Raman experiments. Y.C. supervised the project. All authors contributed to interpretations of the results.

Notes

The authors declare no competing financial interest.

ACKNOWLEDGMENTS

Y.C. acknowledges support from the Assistant Secretary for Energy Efficiency and Renewable Energy, Office of Vehicle Technologies of the U.S. Department of Energy under the Battery Materials Research (BMR) program and Battery 500 Consortium. Yuzhang Li acknowledges the Intelligence Community Fellowship for funding.

REFERENCES

(1) Chu, S.; Majumdar, A. *Nature* **2012**, *488* (7411), 294−303.
(2) Chu, S.; Cui, Y.; Liu, N. *Nat. Mater.* **2017**, *16* (1), 16−22.
(3) Lin, D.; Liu, Y.; Cui, Y. *Nat. Nanotechnol.* **2017**, *12* (3), 194−206.
(4) Liu, Y.; Zhou, G.; Liu, K.; Cui, Y. *Acc. Chem. Res.* **2017**, *50* (12), 2895−2905.
(5) Yan, K.; Lee, H.-W.; Gao, T.; Zheng, G.; Yao, H.; Wang, H.; Lu, Z.; Zhou, Y.; Liang, Z.; Liu, Z.; Chu, S.; Cui, Y. *Nano Lett.* **2014**, *14* (10), 6016−6022.
(6) Zheng, G.; Lee, S. W.; Liang, Z.; Lee, H.-W.; Yan, K.; Yao, H.; Wang, H.; Li, W.; Chu, S.; Cui, Y. *Nat. Nanotechnol.* **2014**, *9* (8), 618−623.
(7) Li, N.-W.; Yin, Y.-X.; Yang, C.-P.; Guo, Y.-G. *Adv. Mater.* **2016**, *28* (9), 1853−1858.
(8) Zheng, G.; Wang, C.; Pei, A.; Lopez, J.; Shi, F.; Chen, Z.; Sendek, A. D.; Lee, H.-W.; Lu, Z.; Schneider, H.; Safont-Sempere, M. M.; Chu, S.; Bao, Z.; Cui, Y. *ACS Energy Lett.* **2016**, *1* (6), 1247−1255.
(9) Liu, W.; Li, W.; Zhuo, D.; Zheng, G.; Lu, Z.; Liu, K.; Cui, Y. *ACS Cent. Sci.* **2017**, *3* (2), 135−140.
(10) Liu, Y.; Lin, D.; Yuen, P. Y.; Liu, K.; Xie, J.; Dauskardt, R. H.; Cui, Y. *Adv. Mater.* **2017**, *29* (10), 1605531.
(11) Zhao, J.; Liao, L.; Shi, F.; Lei, T.; Chen, G.; Pei, A.; Sun, J.; Yan, K.; Zhou, G.; Xie, J.; Liu, C.; Li, Y.; Liang, Z.; Bao, Z.; Cui, Y. *J. Am. Chem. Soc.* **2017**, *139* (33), 11550−11558.
(12) Lin, D.; Liu, Y.; Chen, W.; Zhou, G.; Liu, K.; Dunn, B.; Cui, Y. *Nano Lett.* **2017**, *17* (6), 3731−3737.
(13) Lu, Y.; Tu, Z.; Archer, L. A. *Nat. Mater.* **2014**, *13* (10), 961−969.
(14) Shi, Q.; Zhong, Y.; Wu, M.; Wang, H.; Wang, H. *Proc. Natl. Acad. Sci. U. S. A.* **2018**, *115* (22), 5676−5680.
(15) Li, W.; Yao, H.; Yan, K.; Zheng, G.; Liang, Z.; Chiang, Y.-M.; Cui, Y. *Nat. Commun.* **2015**, *6*, 7436.
(16) Zhang, X.-Q.; Cheng, X.-B.; Chen, X.; Yan, C.; Zhang, Q. *Adv. Funct. Mater.* **2017**, *27* (10), 1605989.
(17) Zhang, X.-Q.; Chen, X.; Cheng, X.-B.; Li, B.-Q.; Shen, X.; Yan, C.; Huang, J.-Q.; Zhang, Q. *Angew. Chem., Int. Ed.* **2018**, *57* (19), 5301−5305.
(18) Li, N.-W.; Yin, Y.-X.; Li, J.-Y.; Zhang, C.-H.; Guo, Y.-G. *Adv. Sci.* **2017**, *4* (2), 1600400.
(19) Cheng, X.-B.; Zhao, M.-Q.; Chen, C.; Pentecost, A.; Maleski, K.; Mathis, T.; Zhang, X.-Q.; Zhang, Q.; Jiang, J.; Gogotsi, Y. *Nat. Commun.* **2017**, *8* (1), 336.
(20) Qian, J.; Henderson, W. A.; Xu, W.; Bhattacharya, P.; Engelhard, M.; Borodin, O.; Zhang, J.-G. *Nat. Commun.* **2015**, *6*, 6362.
(21) Suo, L.; Hu, Y.-S.; Li, H.; Armand, M.; Chen, L. *Nat. Commun.* **2013**, *4*, 1481.
(22) Fan, X.; Chen, L.; Ji, X.; Deng, T.; Hou, S.; Chen, J.; Zheng, J.; Wang, F.; Jiang, J.; Xu, K.; Wang, C. *Chem.* **2018**, *4* (1), 174−185.
(23) Lin, D.; Liu, Y.; Liang, Z.; Lee, H.-W.; Sun, J.; Wang, H.; Yan, K.; Xie, J.; Cui, Y. *Nat. Nanotechnol.* **2016**, *11* (7), 626−632.
(24) Yan, K.; Lu, Z.; Lee, H.-W.; Xiong, F.; Hsu, P.-C.; Li, Y.; Zhao, J.; Chu, S.; Cui, Y. *Nat. Energy* **2016**, *1* (3), 16010.
(25) Liu, L.; Yin, Y.-X.; Li, J.-Y.; Li, N.-W.; Zeng, X.-X.; Ye, H.; Guo, Y.-G.; Wan, L.-J. *Joule* **2017**, *1* (3), 563−575.
(26) Zuo, T.-T.; Wu, X.-W.; Yang, C.-P.; Yin, Y.-X.; Ye, H.; Li, N.-W.; Guo, Y.-G. *Adv. Mater.* **2017**, *29* (29), 1700389.
(27) Liang, Z.; Lin, D.; Zhao, J.; Lu, Z.; Liu, Y.; Liu, C.; Lu, Y.; Wang, H.; Yan, K.; Tao, X.; Cui, Y. *Proc. Natl. Acad. Sci. U. S. A.* **2016**, *113* (11), 2862−2867.
(28) Zhang, R.; Chen, X.; Shen, X.; Zhang, X.-Q.; Chen, X.-R.; Cheng, X.-B.; Yan, C.; Zhao, C.-Z.; Zhang, Q. *Joule* **2018**, *2* (4), 764−777.
(29) Liu, L.; Yin, Y.-X.; Li, J.-Y.; Wang, S.-H.; Guo, Y.-G.; Wan, L.-J. *Adv. Mater.* **2018**, *30* (10), 1706216.
(30) Zuo, T.-T.; Yin, Y.-X.; Wang, S.-H.; Wang, P.-F.; Yang, X.; Liu, J.; Yang, C.-P.; Guo, Y.-G. *Nano Lett.* **2018**, *18* (1), 297−301.
(31) Xie, J.; Wang, J.; Lee, H. R.; Yan, K.; Li, Y.; Shi, F.; Huang, W.; Pei, A.; Chen, G.; Subbaraman, R.; Christensen, J.; Cui, Y. *Sci. Adv.* **2018**, *4* (7), No. eaat5168.
(32) Liu, Y.; Lin, D.; Liang, Z.; Zhao, J.; Yan, K.; Cui, Y. *Nat. Commun.* **2016**, *7*, 10992.
(33) Liang, Z.; Zheng, G.; Liu, C.; Liu, N.; Li, W.; Yan, K.; Yao, H.; Hsu, P.-C.; Chu, S.; Cui, Y. *Nano Lett.* **2015**, *15* (5), 2910−2916.
(34) Wang, S.-H.; Yin, Y.-X.; Zuo, T.-T.; Dong, W.; Li, J.-Y.; Shi, J.-L.; Zhang, C.-H.; Li, N.-W.; Li, C.-J.; Guo, Y.-G. *Adv. Mater.* **2017**, *29* (40), 1703729.

(35) Chi, S.-S.; Liu, Y.; Song, W.-L.; Fan, L.-Z.; Zhang, Q. *Adv. Funct. Mater.* **2017**, *27* (24), 1700348.
(36) Lin, D.; Zhao, J.; Sun, J.; Yao, H.; Liu, Y.; Yan, K.; Cui, Y. *Proc. Natl. Acad. Sci. U. S. A.* **2017**, *114*, 4613.
(37) Wang, H.; Lin, D.; Liu, Y.; Li, Y.; Cui, Y. *Sci. Adv.* **2017**, *3* (9), No. e1701301.
(38) Zhu, Y.; Peng, L.; Fang, Z.; Yan, C.; Zhang, X.; Yu, G. *Adv. Mater.* **2018**, *30* (15), 1706347.
(39) Peng, L.; Fang, Z.; Zhu, Y.; Yan, C.; Yu, G. *Adv. Energy Mater.* **2018**, *8* (9), 1702179.
(40) Wang, H.; Wang, C.; Matios, E.; Li, W. *Nano Lett.* **2017**, *17* (11), 6808−6815.
(41) Yoon, S.-M.; Choi, W. M.; Baik, H.; Shin, H.-J.; Song, I.; Kwon, M.-S.; Bae, J. J.; Kim, H.; Lee, Y. H.; Choi, J.-Y. *ACS Nano* **2012**, *6* (8), 6803−6811.
(42) Li, Y.; Yan, K.; Lee, H.-W.; Lu, Z.; Liu, N.; Cui, Y. *Nat. Energy* **2016**, *1* (2), 15029.
(43) Ohzuku, T.; Iwakoshi, Y.; Sawai, K. *J. Electrochem. Soc.* **1993**, *140* (9), 2490−2498.
(44) Song, X. Y.; Kinoshita, K.; Tran, T. D. *J. Electrochem. Soc.* **1996**, *143* (6), L120−L123.
(45) Dahn, J. R.; Fong, R.; Spoon, M. J. *Phys. Rev. B: Condens. Matter Mater. Phys.* **1990**, *42* (10), 6424−6432.
(46) Li, Y.; Li, Y.; Pei, A.; Yan, K.; Sun, Y.; Wu, C.-L.; Joubert, L.-M.; Chin, R.; Koh, A. L.; Yu, Y.; Perrino, J.; Butz, B.; Chu, S.; Cui, Y. *Science* **2017**, *358* (6362), 506−510.
(47) Suo, L.; Xue, W.; Gobet, M.; Greenbaum, S. G.; Wang, C.; Chen, Y.; Yang, W.; Li, Y.; Li, J. *Proc. Natl. Acad. Sci. U. S. A.* **2018**, *115* (6), 1156−1161.
(48) Liu, S.; Wang, A.; Li, Q.; Wu, J.; Chiou, K.; Huang, J.; Luo, J. *Joule* **2018**, *2* (1), 184−193.
(49) Hafez, A. M.; Jiao, Y.; Shi, J.; Ma, Y.; Cao, D.; Liu, Y.; Zhu, H. *Adv. Mater.* **2018**, *30*, 1802156.
(50) Li, Y.; Li, Y.; Sun, Y.; Butz, B.; Yan, K.; Koh, A. L.; Zhao, J.; Pei, A.; Cui, Y. *Nano Lett.* **2017**, *17* (8), 5171−5178.